DOI: https://doi.org/10.53350/pjmhs2023172706

ORIGINAL ARTICLE

Study and Analysis of the Structural and Magnetic Properties of Nickel Iron Substituted with Different Proportions of Cerium

HASSAN N. MAHMOOD[1], KHALID H. RAZEG[2], SABAH M. ALI RIDHA[3]
[1,2]Tikrit University, College of Education for Pure Science, Physics Department, Iraq
[3]Kirkuk University, College of Education for Pure Science, Physics Department, Iraq
Correspondence to: Hassan N. Mahmood, Email: hassan.n.mahmood@st.tu.edu.iq.

ABSTRACT

Magnetic nanoferrites were prepared from nickel substituted with pure cerium ions by the following formula, $NiCe_xFe_{2-x}O_4$, where (x = 0.00, 0.02, 0.06, 0.08, 0.1) and in different proportions and weights using the chemical sol-gel method, after which it was calcined at 600, 800, and 1000 °C. And by using different characterization methods to examine the prepared powders such as X-ray diffractometer (XRD), scanning electron microscopy (FESEM) and vibration sample magnetometer (VSM). The X-ray diffraction patterns of the prepared samples confirmed the formation of single-phase soft magnetic nanoparticles of spinel nature and measured the particle size by XRD and FESEM analysis. Through, EDS analysis it was confirmed that there are no extra impurities and that the samples are pure. The VSM technique was used to analyze the magnetic properties of the as-prepared composites, and the saturation magnetization (Ms) and coercivity (Hc) decreased with increasing concentration of compensated cerium ions. These properties reveal the highly magnetic nature of cerium-substituted nickel nanoparticles and their potential for use in modern communication technology.

Keywords: Nanoparticles, Nickel ferrites, cerium ion, X-ray diffraction, FESEM analysis, VSM analysis.

INTRODUCTION

In recent years, research's has concentrated on enhancing nanomaterials' structural, electrical, and magnetic characteristics to produce a potential material for a variety of applications [1]. Among these nickel ferrite nanoparticles that lead to specific ferrite, ferrite nanoparticles are currently showing exceptional uses.in biology, engineering, magnetic fluids, high-density data storage, photocatalysts, MRI, and other fields. [2-4]. Due to the presence of certain divalent or trivalent elements during the manufacturing and processing of ferrite nanoparticles, the distribution of metal ions and therefore their characteristics are changed [5]. The standard formula for ferrite nanoparticles, which have a spinel structure, is AB_2O_4 [6]. In spinel iron, the distribution of tetrahedral (a) and octahedral (b) sites changes when metal cations of varying valences are introduced [7]. Due to fact that type of cations distribution at the octahedral and tetrahedral sites in the cubic spinel lattice affects a number of important ferrite spinel characteristics [8, 9]. $NiFe_20_4$ is a soft ferrite with a spinel structure that is inverted. In the inverted spinel structure, 50% of Fe^{+3} ion and all of the X^{2+} ions are located in the B site, while the other half of Fe^{+3} remains in the A site [10], $NiFe_2O_4$ has an inverted spinel structure, which allows Fe^{+3} ions to easily transition between tetrahedral and octahedral sites (A and B) [11]. Any alteration in the distribution of cations between the tetrahedral and octahedral sites has a significant impact on their physical characteristics [12]. Because of its abundance in nature, ferromagnetic behavior that depends on particle size and shape, low eddy current and conductivity, high electrical resistivity, and electrochemical stability, Ni Ferrite is one of the most adaptable and significant soft ferrite materials in terms of technology [13,14].Numerous synthesis methods, such as solid-solids, melt heat, hydrothermal, ball milling, precipitation, wet chemical techniques, and sol-gel, are often used to create spinel iron with nanostructures [15- 20]. The sol-gel method is the most widely used method among chemical synthesis techniques for creating pure rare earth element REE nanoparticles. For this synthesis, we opted for the sol-gel technique of nickel ferrite in the current work due to number of advantages, including ease of work, simple synthesis of nanoparticles with controlled crystal size by controlling pH value, calcination temperature, and a relatively low-cost method when compared to other methods. The sol-gel approach also allows for the observation of strong peaks devoid of contaminants. Ce^{3+} ions have an ionic radius of (1.03 Å), which is greater than of Fe^{3+} ions, which is (0.64 Å) [21], and this produces a drop in saturation magnetization [7], by weakening the sublattice interaction and lowering the unit cells' magnetic moments. As a result, lead to decrease structural factors, including crystal size. These characteristics demonstrate the nickel nanoparticles with cerium substitutions' strong magnetic capabilities, which may be used in contemporary communications technology.

Specifics of experimental

MATERIALS AND METHODS

Cerium-substituted nickel ferrites were converted into nanoparticles using the sol-gel auto combustion technique, $NiCe_xFe_{2-x}O_4$ (x = 0.00, 0.02, 0.04, 0.06, 0.08, 0.1), by making a mixed solution of, cerium nitrate Ce $(NO_3)_3.6H_2O$ (99.8%), nickel nitrate Ni $(NO_3)_2.6H_2O$ (99.8%), ferric nitrate Fe $(NO_3)_3.6H_2O$ (99.8%), and citric acid $C_6H_8O_7$. Where each substance was weighed separately in different proportions and weights and dissolved individually in a specific amount of ionized water and stirred to obtain completely dissolved solutions together, and by adding ammonia solution by distillation in order to change and raise the pH of the resulting solutions to 7 [22]. By gradually raising the temperature of the device to 90 degrees Celsius with continuous stirring for 3 to 4 hours (depending on the type of solution and the proportion and weight of materials), it reaches the gel stage. When the gel was first created, and its temperature rose, at a temperature of about 200 °C, a significant number of gases were released, the gel began to auto-combust, and the gel was then transformed into ferrite powder that had been burned. The resultant as-burned powders were then thermally calcined for 3 hours at 600, 800 and 1000 °C to eliminate organic waste and increase the homogeneity of the samples before being utilized for further structural and magnetic property research.

Characterizations: The crystal structure of the produced samples was studied by X-Ray Diffraction (XRD), outfitted with a high-intensity Cu radiation source (0.154 nm, 40 mA, 40 kV), in the 10°–80° range , step size (2θ):0.0260 . Field Emission Scanning Electron Microscopy (FESEM) was used to analyses the morphology of the calcined powders at 800 °C. By utilizing a model vibrating sample magnetometer (VSM) with an applied field range of (-15000 to +15000) Oe at ambient temperatures. The magnetic characteristics of powders calcined at 800 °C were investigated using a vibrating sample magnetometer.

RESULTS AND DISCUSSION

Structural Analysis: Figure 1 shows the XRD patterns of nickel ferrite substituted with cerium ions (x = 0.00, 0.02, 0.04, 0.06, 0.08, and 0.1) for the particles that have been calcined and burned at various temperatures at 600, 800, and 1000 °C. Where the XRD patterns show that all reflection peaks belong to (220), (311), (222), (400), (422), (511), and (440) for all pure samples compensated with cerium ions, these peaks positions of the XRD

patterns match with the traditional patterns of reference code 01-074-2081 for pure $NiFe_2O_4$ and 98-011-1373 for Ce-substituted $NiCe_xFe_{2-x}O_4$, Some of the peaks marked with an asterisk (*) may be due to the presence of hematite as a result of complete non-incombustion, but all the main peaks belonging to the pure single spinel phase remained unchanged as a result of the substitution and confirmed the appearance of the spinel phase. Our results show that the diffraction peaks sharpen and decrease with the increase in the sintering temperature, and their intensity also increases, indicating that the crystallization is condensed as a result of the increase in the crystal size ratio resulting from the larger core size of the ions substituted [23].

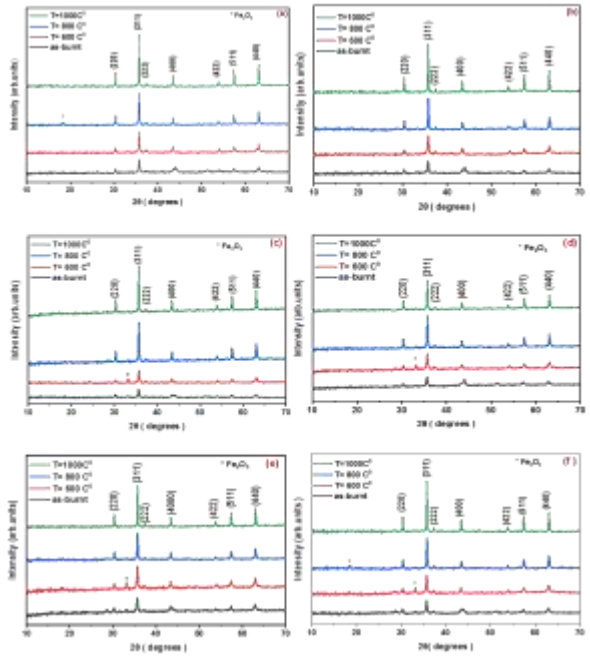

Fig.1: XRD shapes $NiCe_xFe_{2-x}O_4$ (a-f) x= (0.00, 0.02, 0.04, 0.06, 0.08, 0.1)

Using Scherrer's formula, to determine crystallite size (D) of each sample. The density (ρ_x), lattice constant (a), and hop length in A-site (L_A) tetrahedral and B-site (L_B) octahedral crystals were estimated using the equation indicated below [24- 28].

$$D = \frac{0.96\,\lambda}{\beta \cos\theta} \qquad (1)$$

λ, X-ray wavelength , β : total width at the midpoint of maximum of respective peak.

$$\rho_x = \frac{8M}{Na^3} \qquad (2)$$

M: compound's molecular weight, N: Avogadro's number.

$$a = d_{hkl}\sqrt{h^2 + k^2 + l^2} \qquad (3)$$

d: distance between planes, (h, k, l) Miller's coefficients.

$$L_A = a\frac{\sqrt{3}}{4} \qquad (4)$$

$$L_B = a\frac{\sqrt{2}}{4} \qquad (5)$$

We note from the data presented in Table 1, derived from the above equations, that the crystal size (D) values of the pure unsubstituted samples (x = 0.00) are higher than those of the other partially substituted samples. As the Ce-substitution increases, the crystal size (D) value continues to decrease. The same trend was observed in the crystallite size variation in chromium-substituted ferric magnesium and chromium-substituted nickel ferrite [29]. We also note from the table that by increasing the amount of Ce substitution in the samples, the crystal size decreases because the substitution ions hinder the formation of crystal grains. Also, with higher calcination temperatures, the crystallite size increases because a higher calcination temperature lowers the specific particle surface area, which is largely consistent with previous studies [30]. The values of lattice constant (a) that we obtained are also tabulated in Table 1, and it is known that lattice parameters are affected by several factors, such as interaction forces between atoms, size of atoms, final sizes, and others. [31]. The values of the lattice constant (a) obtained at the calcination temperatures of 600, 800 and 1000 °C were found to be nearly constant, with a very slight increase at increasing compensation by Ce^{3+} ions and higher calcination temperature, indicating that the RER substitution did not cause much distortion in the components lattice, which is largely consistent with previous studies [30], may be due to the very slight increase due to the fact the radius of the Fe^{3+} ions (0.64 Å) is less than the radius of the substituted Ce^{3+} ions (1.03 Å). While the increase in the rate of substitution of cerium in solution leads to a change in the positions of both the tetrahedron and the octahedron [7]. From equation (2), we note that the X-ray intensity (ρ_x) depends on the compound's molar mass and lattice parameter (a), as shown in Table 1, for the calcination temperatures of 600, 800, and 1000 °C, with decreasing weight Molecular, the values of (ρ_x) decrease in an almost linear fashion. This is likely caused by the lower atomic weight of nickel compared to cerium. The resulting increase in the jump length L between magnetic ions modifies the physical properties of ferrite. [32]. Table 1 presents the results of the calculations made to determine the (L_A) and (L_B) jump lengths for all samples, which were calculated from equations (4,5).

Table 1: (D) crystallite size, (a) lattice constant, (ρx) density of x-ray, hopping length: Value for $NiCe_xFe_{2-x}O_4$, x= 0.00, 0.02, 0.04, 0.06, 0.08, 0.1

x	compositions	Temp °C	D mn	Aa	ρ_x gm/cm^3	L_A A^0	L_B A^0
0.00	$NiFe_2O_4$	as- burnt	31.643	8.324	5.29	3.604	2.943
		600	33.857	8.334	5.38	3.608	2.946
		800	42.657	8.337	5.37	3.609	2.947
		1000	51.174	8.339	5.38	3.610	2.948
0.02	$NiCe_{0.02}Fe_{1.98}O_4$	as- burnt	27.300	8.321	5.32	3.603	2.941
		600	26.621	8.326	5.34	3.605	2.943
		800	38.444	8.335	5.34	3.609	2.946
		1000	51.183	8.336	5.32	3.609	2.947
0.04	$NiCe_{0.04}Fe_{1.96}O_4$	as- burnt	26.870	8.321	5.37	3.603	2.941
		600	27.247	8.327	5.34	3.605	2.944
		800	39.488	8.331	5.38	3.607	2.945
		1000	46.800	8.334	5.38	3.608	2.946
0.06	$NiCe_{0.06}Fe_{1.94}O_4$	as- burnt	23.850	8.322	5.32	3.603	2.942
		600	25.200	8.333	5.30	3.608	2.946
		800	38.692	8.333	5.32	3.608	2.946
		1000	43.884	8.338	5.32	3.610	2.947
0.08	$NiCe_{0.08}Fe_{1.92}O_4$	as- burnt	24.373	8.321	5.27	3.603	2.941
		600	27.857	8.333	5.32	3.608	2.946
		800	36.302	8.334	5.32	3.608	2.946

		1000	49.229	8.336	5.32	3.609	2.947
0.1	$NiCe0.1Fe_{1.9}O_4$	as- burnt	25.642	8.323	5.30	3.603	2.942
		600	26.057	8.333	5.32	3.608	2.946
		800	35.358	8.334	5.32	3.608	2.946
		1000	48.229	8.336	5.32	3.609	2.947

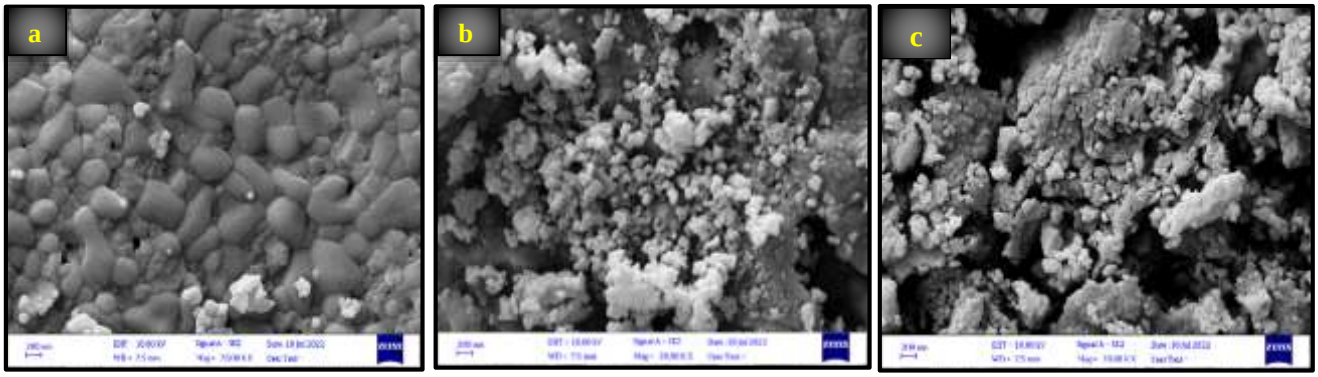

.
Fig. 2: FESEM images, a) x=0.00, b) x = 0.06, c) x=0.1, for $NiCe_xFe_{2-x}O_4$ samples

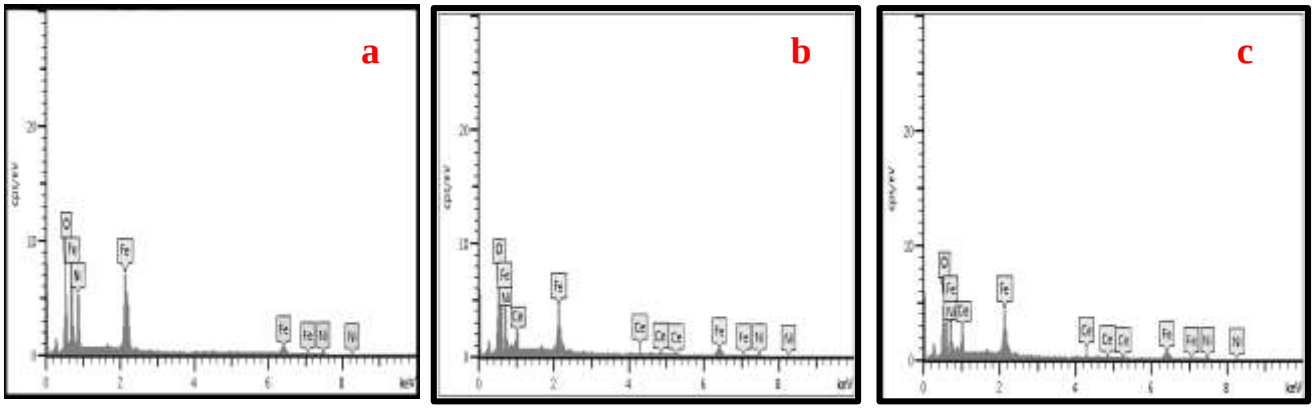

Fig. 3: EDS spectra a) x=0.00, b) x = 0.06, c) x=0.1, for $NiCe_xFe_{2-x}O_4$ samples calcined at 800 ˚C

FESEM Analysis: An FE-SEM examination was performed to study the surface shape and particle size of Ce-substituted ferrite nanoparticles (x = 0.0, 0.4, 1.0) calcined at 800 °C to ensure the initial composition the samples produced using EDS spectra obtained during FE-SEM analysis. From Fig. 2(a–c), we note the substitution with the Ce^{3+} ion has a significant effect on the grain morphology, particle size, shape, uniformity, homogeneity, and distribution, as cerium substituted grains adhere uniformly to the surface of the nickel ferrite nanoparticles. From the image of sample 2(a) unsubstituted with cerium ions, we note the heterogeneity and composition of the porous structure and polyhedrons, revealing relatively larger, irregular, and non-uniform crystal sizes. It's possible that the combustion process's surplus gas emissions are what caused the heterogeneity and the construction of the porous structure [33]. Whereas in Fig. 2(b–c), the surrogate samples show homogenous nanoscale particle size distribution, spherical shape, and homogeneous microstructure, where the interaction between the magnetic nanoparticles and the calcination temperature, which occurs naturally, caused the formation of certain lumpy regions in the FESEM images, In many cases of nano spinels, it has been observed that the nanoparticles tend to stick together [34], and the average particle size continues to decrease with increasing replacement of Ce^{3+} ions, as shown in Table1. Increased compensation of ions leads to a decrease in particle size, which is what largely agrees with previous studies [2, 9]

calcined at 800 ˚C.

We note from Table 2 that there is a fairly good agreement in the particle size for FESEM analysis with the particle size calculated for XRD. Also, molecular structural disorder and lattice strain, which are caused by different ionic radii or nanoparticle clustering, may explain the small difference between the particle sizes calculated by FESEM for the current samples and those obtained from relation (1). As is known, XRD analysis is more rigorous and yields smaller volumes [35, 36].

Table 2: Average crystallite size of XRD and FESEM, x= 0.00, 0.06, 0.1 for $NiCe_xFe_{2-x}O_4$ samples calcined at 800 ˚

x	compositions	XRD, D (nm)	FESEM, D (nm)
0.00	$NiFe_2O_4$	42.657	55.955
0.06	$NiCe_{0.06}Fe_{1.94}O_4$	38.692	43.163
0.1	$NiCe_{0.1}Fe_{1.9}O_4$	35.358	40.243

As for the EDS spectra shown in Fig. 3, the pure samples as well as the samples with different concentration of cerium proved the validity of their elemental composition and the absence of excess impurities in them. So in the present work, we note the purity of the prepared nanoparticles.

VSM Analysis: A vibrational magnetometer analysis (VSM) was performed to determine the magnetic properties of synthesized $NiCe_xFe_{2-x}O_4$ nanoparticles (x = 0.00, 0.02, 0.04, 0.06, 0.08, 0.1) calcined at 800°C in ambient temperatures. As shown in the figure (4) in the applicable field ranging from (-15000 to +15000) Oe. Where we notice an S-shaped curve for ferrite nanoparticles,

magnetic parameters such as saturation magnetization (Ms), coercive force (Hc), remanent magnetization (Mr), magnetic moment (n_B), and magnetic anisotropy (K), were calculated using magnetic hysteresis loops (MH) and special relations.

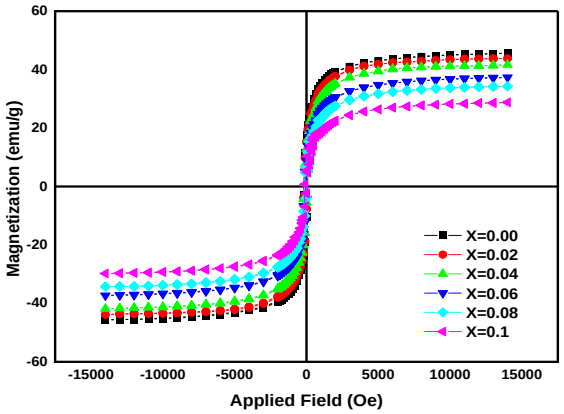

Fig.4: Magnetic hysteresis curve x = 0.00, 0.02, 0.04 0.06, 0.08, 0.1, $NiCe_xFe_{2-x}O_4$, samples calcined at 800 ˚C.

The results are presented in the table (3), where we notice that cerium ions substituted with different concentrations in the ferrite nickel network have caused remarkable changes in the magnetic properties. According to the table (3), value of saturation magnetization (Ms) decrease when increasing cerium substitution in the nickel ferrite network, as indicated MH magnetic hysteresis rings, as the value of (Ms) for the pure compound (x = 0) is (44.574 emu / g) and decreased with increasing cerium content (x = 0.1) to (28.711 emu/g) because Ce^{3+} ions replace iron ions, lower the magnetic moments of the unit cells and diminish the sub-lattice interaction. Since the Ce3+ ion is non-magnetic, this decrease in Ms with increased Ce substitution may be linked to the cations distribution between the spinel structure's A and B sites., which is consistent with previous reports [2, 24, 30], where the saturation magnetization strongly depends on the disorder of the cations and the interaction of the magnetic exchange on the octahedral and tetrahedral sites of the lattice [30, 37]. According to this study, compared with the original ferrite sample, cerium substitution reduced the saturation magnetization of nickel ferrite. The values of coercive force (Hc) were found for ferrites prepared from the hysteresis ring and as seen in Table (3), for the pure compound $NiCe_xF_2O_4$ at x = 0, it is (180.237 Oe). It decreases in the substituted compound $NiCe_xFe_{2-x}O_4$ at x = 0.1 to (125.946 Oe), which is in agreement with previous reports [2, 5, 38]. The drop in the prepared samples' coercive valuesis caused by exchange interaction between A - B, which leads to the occurrence of spin oscillation on the surface of the nanostructures and, in turn, leads to a decrease in magnetism the ferrite nanosamples , thus, drastic changes for saturation magnetization occur in A-B exchange reactions [39, 40]. The values of residual magnetization (Mr) are found in the hysteresis loop, and Mr is the residual magnetization in ferromagnetic materials after removing the external magnetic field. And its value for the unsubstituted pure ferrite compounds at (x = 0) was 17.783 emu/g, and the value of the substituted compound at (x = 0.1) decreased to 5.451 emu/g.

Table 3: Values of (Ms, Mr, Hc, n_B, Mr/Ms ratio and K) x = 0.00, 0.06, 0.1, NiCexFe2-xO4 samples calcined at 800 ˚C.

x	M_s (emu/g)	M_r (emu/g)	H_c (Oe)	n_B (μ_B)	Mr / Ms	K × 10^3 emu/Oeg
0.00	44.574	17.783	180.237	1.87	0.40	8.37
0.02	43.757	15.222	172.253	1.85	0.35	7.85
0.04	41.577	12.845	163.642	1.77	0.31	7.09
0.06	37.324	8.866	142.402	1.60	0.24	5.54
0.08	34.242	6.712	136.055	1.47	0.20	4.85
0.1	28.711	5.451	125.946	1.24	0.19	3.77

So is the ratio (Mr/Ms) which an important distinguishing parameter for ferromagnetic applications, when this ratio is less than 0.5, the particles interact via magnetic interactions, and the interaction is reciprocal when this ratio is higher than 0.5 [39, 41]. Similar results are observed for the replacement of nickel ferrite with rare earth [39] ions. In our study, the square ratio values were less than 0.5, indicating that the particles interact through magnetic interactions. Using the following equations, we were able to figure out the magnetic moment (n_B) and the magnetic anisotropy (K) [24].

$$n_B = \frac{M * M_S}{5585} \qquad (6)$$

$$K = \frac{M_S * H_c}{0.96} \qquad (7)$$

Where (M) are the molecular weights of the prepared ferrite compounds. As we can see from the table (3) values of each of the magnetic moment (n_B) and magnetic anisotropy (K) continue to decline when replacement increases of cerium ions in nickel ferrites, this decrease was observed in a previous study [39]. In general, the magnetic parameter of REE depends on the grain size, the exchange of magnetic interactions [42]. With the replacement of cerium ions in nickel ferrite, the magnetic lattice of Fe-O-Fe, which is occupies by the nonmagnetic cerium atom, are disrupted leading to an increase in lattice stress as the magnetic nature depend concentrate of the compensated ions and the variable particle size, resulting in A decrease in the diameter of the crystal and a decrease in magnetic saturation, and the magnetization tends to decrease by compensation as it weakens the exchange. The magnetic moment decrease reason the magnetic properties of smaller particles tend to decrease with an increase in the surface spin fraction and a decrease in saturation magnetization [43].

CONCLUSION

Nanoparticles of nickel that were compensated with pure cerium ions were prepared with the following formula, $NiCe_xFe_{2-x}O_4$, where x = 0.00, 0.02, 0.06, 0.08, 0.1, and with different weights using the sol-gel technique, and calcined at 600, 800, and 1000 °C. Different methods were used to examine powders and analyze composite samples, such as XRD, FESEM, and VSM. Where the results show the formation of single-phase soft nanoparticles that have the nature of spinel, and the size of the particles has been confirmed through XRD and FESEM analysis, as well as the closeness of the values between them. Through EDS analysis, it has been confirmed that there are no impurities and the samples are pure. Saturation magnetization (Ms), residual magnetization (Mr), and coercivity (Hc) decrease with increasing cerium ions concentration which is compensated through the VSM technique to analyze the magnetic properties of the produced composites. These properties reveal the highly magnetic nature of cerium-substituted nickel nanoparticles that can be utilized in modern communications technology.

REFERENCES

1. Dippong, T., Levei, E.A. and Cadar, O., 2021. Recent advances in synthesis and applications of MFe2O4 (M= Co, Cu, Mn, Ni, Zn) nanoparticles. Nanomaterials 11 (6), p.1560.
2. Abhishek, M., Manjunatha, K., Angadi, V.J., Melagiriyappa, E., Anandaram, B.N., Jayanna, H.S., Veena, M. and Acharya, K.S., 2020. Structural and magnetic properties of Eu3+ substituted Mg-Cd nanoferrites: a detailed study of influence of high energy γ-rays irradiation. Chemical Data Collections, 28, p.100460.
3. Dhiman, P., Rana, G., Alshgari, R.A., Kumar, A., Sharma, G., Naushad, M. and ALOthman, Z.A., 2023. Magnetic Ni–Zn ferrite anchored on g-C3N4 as nano-photocatalyst for efficient photo-degradation of doxycycline from water. Environmental Research, 216, p.114665.
4. Rabi, B., Essoumhi, A., Sajieddine, M., Greneche, J.M., Hlil, E.K., Razouk, A. and Valente, M.A., 2020. Structural, magnetic and magnetocaloric study of Ni0. 5Zn0. 5Fe2O4 spinel . Applied Physics A , 126(3), pp.1-11.
5. Prathapani, S., Jayaraman, T.V., Varaprasadarao, E.K. and Das, D., 2014. Structural and ambient/sub-ambient temperature magnetic properties of Er-substituted cobalt-ferrites synthesized by sol-gel assisted auto-combustion method. Journal of Applied Physics , 116(2), p.023908.

6. Chakradhary, V.K., Ansari, A. and Akhtar, M.J., 2019. Design, synthesis, and testing of high coercivity cobalt doped nickel ferrite nanoparticles for magnetic applications. Journal of Magnetism and Magnetic Materials , 469, pp.674-680.
7. Mohammad, A.M., Aliridha, S.M. and Mubarak, T.H., 2018. STRUCTURAL AND MAGNETIC PROPERTIES OF Mg-Co FERRITE NANOPARTICLES . Digest Journal of Nanomaterials & Biostructures (DJNB), 13(3).
8. Vadivel, M., Babu, R.R., Sethuraman, K., Ramamurthi, K. and Arivanandhan, M., 2014. Synthesis, structural, dielectric, magnetic and optical properties of Cr substituted CoFe2O4 nanoparticles by co-precipitation method. Journal of magnetism and magnetic materials , 362, pp.122-129.
9. Mohammad, A.M., Ridha, S.M.A. and Mubarak, T.H., 2018. Dielectric properties of Cr-substituted cobalt ferrite nanoparticles synthesis by citrate-gel auto combustion method . Int. J. Appl. Eng . Res, 13(8) , pp.6026-6035.
10. Elayakumar, K., Sathana, V. and Kumar, R.T., 2020. Structural and magnetic characterization of rare earth element cerium-doped nickel ferrite nanoparticles (NiCexFe2-xO4) by sol-gel method with antibacterial activity. Journal of Superconductivity and Novel Magnetism, 33(7), pp.2171-2178.
11. Feng, S., Yang, W. and Wang, Z., 2011. Synthesis of porous NiFe2O4 microparticles and its catalytic properties for methane combustion . Materials Science and Engineering: B, 176(18), pp.1509-1512.
12. Gharibshahian, M., Mirzaee, O. and Nourbakhsh, M.S., 2017. Evaluation of superparamagnetic and biocompatible properties of mesoporous silica coated cobalt ferrite nanoparticles synthesized via microwave modified Pechini method. Journal of Magnetism and Magnetic Materials, 425, pp.48-56.
13. Ravichandran, A.T., Srinivas, J., Karthick, R., Manikandan, A. and Baykal, A., 2018. Facile combustion synthesis, structural, morphological, optical and antibacterial studies of Bi1− xAlxFeO3 (0.0≤ x≤ 0.15) nanoparticles. Ceramics International , 44(11), pp.13247-13252.
14. Shanmugavel, T., Raj, S.G., Rajarajan, G. and Kumar, G.R., 2014. Tailoring the structural and magnetic properties and of nickel ferrite by auto combustion method. Procedia materials science , 6, pp.1725-1730.
15. Sudheesh, V.D., Thomas, N., Roona, N., Choudhary, H., Sahoo, B., Lakshmi, N. and Sebastian, V., 2018. Synthesis of nanocrystalline spinel ferrite (MFe2O4, M= Zn and Mg) by solution combustion method: influence of fuel to oxidizer ratio. Journal of Alloys and Compounds , 742, pp.577-586.
16. Anantharamaiah, P.N., Shashanka, H.M., Kumar, R., Chelvane, J.A. and Sahoo, B., 2021. Chemically enabling CoFe2O4 for magnetostrictive strain sensing applications at lower magnetic fields : Effect of Zn substitution. Materials Science and Engineering: B, 266, p.115080.
17. Anantharamaiah, P.N., Rao, B.P., Shashanka, H.M., Chelvane, J.A., Khopkar, V. and Sahoo, B., 2021. Role of Mg 2+ and In 3+ substitution on magnetic, magnetostrictive and dielectric properties of NiFe 2 O 4 ceramics derived from nanopowders. Physical Chemistry Chemical Physics , 23(2), pp.1694-1705.
18. Bhandare, S.V., Kumar, R., Anupama, A.V., Choudhary, H.K., Jali, V.M. and Sahoo, B., 2020. Mechanistic insights into the sol-gel synthesis of complex (quaternary) Co–Mn–Zn-spinel ferrites: An annealing dependent study. Ceramics International , 46(11), pp.17400-17415.
19. Bhandare, S.V., Kumar, R., Anupama, A.V., Mishra, M., Kumar, R.V., Jali, V.M. and Sahoo, B., 2020. Effect of Mg-substitution in Co–Ni-Ferrites: Cation distribution and magnetic properties. Materials Chemistry and Physics , 251, p.123081.
20. Thomas, N., Sudheesh, V.D., Choudhary, H.K., Sahoo, B., Nair, S.S., Lakshmi, N. and Sebastian, V., 2019. Magnetic properties of MFeCrO4 (M= Co/Ni) prepared by solution combustion method. Journal of Superconductivity and Novel Magnetism , 32(9), pp.2973-2979.
21. Kumar, K.V., Bhavani, S.D. and Shukur, M.A., 2022. The Study of Temperature Dependent Structural and Elastic Properties of . Bulgarian Journal of Physics, 20(20XX), pp.1-16.
22. Sobhani-Nasab, A., Ziarati, A., Rahimi-Nasrabadi, M., Ganjali, M.R. and Badiei, A., 2017. Five-component domino synthesis of tetrahydropyridines using hexagonal PbCr x Fe12− x O19 as efficient magnetic nanocatalyst . Research on Chemical Intermediates , 43(11), pp.6155-6165.
23. Chakrabarty, S., Pal, M. and Dutta, A., 2015. Structural, optical and electrical properties of chemically derived nickel substituted zinc ferrite nanocrystals. Materials Chemistry and Physics , 153, pp.221-228.
24. Anwar, A., Zulfiqar, S., Yousuf, M.A., Ragab, S.A., Khan, M.A., Shakir, I. and Warsi, M.F., 2020. Impact of rare earth Dy+ 3 cations on the various parameters of nanocrystalline nickel spinel ferrite . Journal of Materials Research and Technology , 9(3), pp.5313-5325.
25. Revathi, J., Abel, M.J., Archana, V., Sumithra, T. and Thiruneelakandan, R., 2020. Synthesis and characterization of CoFe2O4 and Ni-doped CoFe2O4 nanoparticles by chemical Co-precipitation technique for photo-degradation of organic dyestuffs under direct sunlight . Physica B: Condensed Matter, 587, p.412136.
26. Li, X., Sun, Y., Zong, Y., Wei, Y., Liu, X., Li, X., Peng, Y. and Zheng, X., 2020. Size-effect induced cation redistribution on the magnetic properties of well-dispersed CoFe2O4 nanocrystals. Journal of Alloys and Compounds , 841, p.155710.
27. Nama, H.K., Venkatesh, N., Ravinder, D., Batoo, K.M., Raslan, E.H. and Hadi, M., 2021. High-Temperature Electrical Properties of Cerium Doped Ni-Zn Nano Ferrites.
28. Javed, T., Maqsood, A. and Malik, A.A., 2011. Structural, electrical and dielectric properties of Co–Mn spinel nanoferrites prepared by co-precipitation technique . Journal of superconductivity and novel magnetism , 24(7), pp.2137-2144.
29. Hankare, P.P., Vader, V.T., Patil, N.M., Jadhav, S.D., Sankpal, U.B., Kadam, M.R., Chougule, B.K. and Gajbhiye, N.S., 2009. Synthesis , characterization and studies on magnetic and electrical properties of Mg ferrite with Cr substitution. Materials Chemistry and Physics , 113(1), pp.233-238.
30. Sonia, M., Anand, S., Vinosel, V.M., Asisi Janifer, M. and Pauline, S., 2018. Effect of lattice strain on structural, magnetic and dielectric properties of sol–gel synthesized nanocrystalline Ce3+ substituted nickel ferrite. Journal of Materials Science: Materials in Electronics, 29(17), pp.15006-15021.
31. Uday Bhasker, S. and Reddy, R. , 2015. Effect of chromium substitution on structural , magnetic and electrical properties of magneto-ceramic cobalt ferrite nano-particles. Journal of Sol-Gel Science and Technology , 73(2), pp.396-402.
32. Sridhar, R., Dachepalli, R. and K Vijaya, K., 2012. Synthesis and characterization of copper substituted nickel nano-ferrites by citrate-gel technique. Advances in Materials Physics and Chemistry, 2012.
33. Gowreesan, S. and Ruban Kumar, A., 2017. Effects of Mg2+ ion substitution on the structural and electric studies of spinel structure of Co1− xMgxFe2O4. Journal of Materials Science: Materials in Electronics, 28(6), pp.4553-4564.
34. Naseri, M.G., Saion, E.B., Ahangar, H.A. and Shaari, A.H., 2013. Fabrication, characterization, and magnetic properties of copper ferrite nanoparticles prepared by a simple , thermal-treatment method. Materials Research Bulletin , 48(4), pp.1439-1446.
35. Ragupathi, C., Vijaya, J.J., Kennedy, L.J. and Bououdina, M., 2014. Combustion synthesis , structure, magnetic and optical properties of cobalt aluminate spinel nanocrystals. Ceramics International , 40(8), pp.13067-13074.
36. Sujatha, C., Reddy, K.V., Babu, K.S., Reddy, A.R. and Rao, K.H., 2012. Effects of heat treatment conditions on the structural and magnetic properties of MgCuZn nano ferrite . Ceramics international , 38(7), pp.5813-5820.
37. Akhtar, M.N., Javed, S., Ahmad, M., Sulong, A.B. and Khan, M.A., 2020. Sol gel derived MnTi doped Co2 W-type hexagonal ferrites: structural, physical, spectral and magnetic evaluations. Ceramics International , 46(6), pp.7842-7849.
38. Akhtar, M.N., Yousaf, M., Lu, Y., Khan, M.A., Sarosh, A., Arshad, M., Niamat, M., Farhan, M., Ahmad, A. and Khallidoon, M.U., 2021. Physical, structural, conductive and magneto-optical properties of rare earths (Yb, Gd) doped Ni–Zn spinel nanoferrites for data and energy storage devices. Ceramics International, 47(9) , pp.11878-11886.
39. Abraham, A.G., Manikandan, A., Manikandan, E., Jaganathan, S.K., Baykal, A. and Renganathan, P., 2017. Enhanced opto-magneto properties of Ni x Mg1–x Fe2O4 (0.0≤ x≤ 1.0) ferrites nano-catalysts. Journal of Nanoelectronics and Optoelectronics, 12(12) , pp.1326-1333.
40. Asiri, S., Sertkol, M., Guner, S., Gungunes, H., Batoo, K.M., Saleh, T.A., Sozeri, H., Almessiere, M.A., Manikandan, A. and Baykal, A., 2018. Hydrothermal synthesis of CoyZnyMn1-2yFe2O4 nanoferrites: magneto-optical investigation. Ceramics International , 44(5), pp.5751-5759.
41. Druc, A.C., Dumitrescu, A.M., Borhan, A.I., Nica, V., Iordan, A.R. and Palamaru, M.N., 2013. Optimization of synthesis conditions and the study of magnetic and dielectric properties for MgFe2O4 ferrite . Central European Journal of Chemistry, 11(8) , pp.1330-1342.
42. Akhtar, M.N., Nazir, M.S., Tahir, Z., Qamar, S. and Khan, M.A., 2020. Impact of Co doping on physical, structural, microstructural and magnetic features of MgZn nanoferrites for high frequency applications. Ceramics International , 46(2), pp.1750-1759.
43. Murthy, Y.L.N., Viswanath, I.K., Rao, T.K. and Singh, R., 2009. Synthesis and characterization of nickel copper ferrite. International Journal of ChemTech Research, 1(4), pp.1308-1311.